

# RSC Advances



This is an *Accepted Manuscript*, which has been through the Royal Society of Chemistry peer review process and has been accepted for publication.

*Accepted Manuscripts* are published online shortly after acceptance, before technical editing, formatting and proof reading. Using this free service, authors can make their results available to the community, in citable form, before we publish the edited article. This *Accepted Manuscript* will be replaced by the edited, formatted and paginated article as soon as this is available.

You can find more information about *Accepted Manuscripts* in the [Information for Authors](#).

Please note that technical editing may introduce minor changes to the text and/or graphics, which may alter content. The journal's standard [Terms & Conditions](#) and the [Ethical guidelines](#) still apply. In no event shall the Royal Society of Chemistry be held responsible for any errors or omissions in this *Accepted Manuscript* or any consequences arising from the use of any information it contains.

**Enhanced lithium storage property of Na-doped  $\text{Li}_2\text{Na}_2\text{Ti}_6\text{O}_{14}$  anode materials  
for secondary lithium-ion batteries**

*Mengmeng Lao, Peng Li, Xiaoting Lin, Lianyi Shao, Miao Shui\*, Nengbing Long,  
Dongjie Wang, Jie Shu\**

*Faculty of Materials Science and Chemical Engineering, Ningbo University, Ningbo  
315211, Zhejiang Province, People's Republic of China*

\* Corresponding author: Jie Shu

Tel.: +86-574-87600787

Fax: +86-574-87609987

E-mail: [sergio\\_shu@hotmail.com](mailto:sergio_shu@hotmail.com) and [shujie@nbu.edu.cn](mailto:shujie@nbu.edu.cn)

\* Corresponding author: Miao Shui

E-mail: [shuimiao@nbu.edu.cn](mailto:shuimiao@nbu.edu.cn)

## Abstract

In this paper, a series of Na-doped  $\text{Li}_2\text{Na}_2\text{Ti}_6\text{O}_{14}$  samples are synthesized by a simple solid-state reaction method through Li-site substitution with Na. Morphology observation shows that all the five materials are well crystallized with a particle size in the range of 150-300 nm. Electrochemical analysis shows that  $\text{Li}_{1.95}\text{Na}_{2.05}\text{Ti}_6\text{O}_{14}$  exhibits lower charge/discharge polarization (0.05 V) than that (0.11 V) of other  $\text{Li}_{2-x}\text{Na}_{2+x}\text{Ti}_6\text{O}_{14}$  samples ( $x=0.00, 0.10, 0.15, 0.20$ ). As a result,  $\text{Li}_{1.95}\text{Na}_{2.05}\text{Ti}_6\text{O}_{14}$  owns the highest initial charge capacity of  $243.6 \text{ mAh g}^{-1}$ , and maintains the reversible capacity of  $210.7 \text{ mAh g}^{-1}$  after 79 cycles. For comparison,  $\text{Li}_{2-x}\text{Na}_{2+x}\text{Ti}_6\text{O}_{14}$  ( $x=0.00, 0.10, 0.15$  and  $0.20$ ) samples only hold the reversible capacity of 159.1, 203.5, 190.1 and  $156.7 \text{ mAh g}^{-1}$ , respectively. Moreover,  $\text{Li}_{1.95}\text{Na}_{2.05}\text{Ti}_6\text{O}_{14}$  also delivers the best rate performance compared with other four samples, with the charge capacity of  $221.1 \text{ mAh g}^{-1}$  at  $200 \text{ mA g}^{-1}$ ,  $211.9 \text{ mAh g}^{-1}$  at  $300 \text{ mA g}^{-1}$ , and  $198.7 \text{ mAh g}^{-1}$  at  $400 \text{ mA g}^{-1}$ . Besides, the reversible in situ structural evolution proves that  $\text{Li}_{1.95}\text{Na}_{2.05}\text{Ti}_6\text{O}_{14}$  is stable host for lithium storage. All the improved electrochemical properties of Na-doped  $\text{Li}_2\text{Na}_2\text{Ti}_6\text{O}_{14}$  should be attributed to the Na-doping with low content, which reduces the charge/discharge polarization and improves the ionic conductivity.

**Keywords:**  $\text{Li}_2\text{Na}_2\text{Ti}_6\text{O}_{14}$ ; Na Doping; Electrochemical behavior; Anode material; Lithium ion batteries.

## 1. Introduction

Because of high energy density, high output working potential and long cycling life, the rechargeable lithium ion batteries have been widely used in portable equipment, such as electric vehicles, hybrid electric vehicles and plug-in hybrid electric vehicles [1, 2]. But the intrinsically poor safety characteristics hinder the large scale deployment of lithium ion batteries. One safety issue is that the dendritic lithium may grow on the surface of anode at high rates due to low Li insertion potential of conventional graphite materials approaching 0.0 V versus Li/Li<sup>+</sup> [3].

To replace the carbonous materials, various titanium based oxides have been proposed as high performance anode materials for lithium ion batteries [4-9]. Compared to widely reported Li<sub>4</sub>Ti<sub>5</sub>O<sub>12</sub>, Li<sub>2</sub>MTi<sub>6</sub>O<sub>14</sub> (M = Sr, Ba, Pb) are a novel kind of hosts for lithium storage [10-14]. The stable framework, lower resistivity and lower working potential (1.4 V versus 1.55 V of Li<sub>4</sub>Ti<sub>5</sub>O<sub>12</sub>,) attract the materials scientists all over the world to make this compound become a promising lithium storage anode material. For instance, the solid state formation mechanism of Li<sub>2</sub>SrTi<sub>6</sub>O<sub>14</sub> anode is investigated using starting materials of SrCO<sub>3</sub>, Li<sub>2</sub>CO<sub>3</sub>, and anatase TiO<sub>2</sub> by ex situ X-ray diffraction (XRD) [10]. It is found that the optimal calcination parameter to form pure Li<sub>2</sub>SrTi<sub>6</sub>O<sub>14</sub> is 950 °C for 8 h. To improve the packing density, mesoporous TiO<sub>2</sub> brookite is used as a template and reactant in a sol-gel synthesis [11]. As a result, Li<sub>2</sub>SrTi<sub>6</sub>O<sub>14</sub> anode shows impressive performance with a reversible capacity of 120 mAh g<sup>-1</sup> at C/14 rate and 92.0 mAh g<sup>-1</sup> at 4C rate.

Isostructural to  $\text{Li}_2\text{SrTi}_6\text{O}_{14}$ ,  $\text{Li}_2\text{Na}_2\text{Ti}_6\text{O}_{14}$  reveals lower lithiation potential of 1.25 V with open channels in the structure enabling the reversible insertion of lithium ions [15-19]. Although  $\text{Li}_2\text{Na}_2\text{Ti}_6\text{O}_{14}$  can be obtained at 600 °C by sol-gel method, it shows a low reversible capacity of about 75 mAh g<sup>-1</sup> [15]. To find appropriate preparation parameters, a comparison between sol-gel route and solid state method is undertaken for  $\text{Li}_2\text{Na}_2\text{Ti}_6\text{O}_{14}$  at different sintering temperatures [16]. It can be found that  $\text{Li}_2\text{Na}_2\text{Ti}_6\text{O}_{14}$  prepared by sol-gel method at 700 °C reveals the highest initial charge specific capacity of 106.6 mAh g<sup>-1</sup> and the best rate properties than any other samples. To further improve the electrochemical properties, the coating by conductive additives, such as copper/carbon, carbon nanotube, graphene, carbon black, is made on  $\text{Li}_2\text{Na}_2\text{Ti}_6\text{O}_{14}$  [17, 18]. As a result, modified  $\text{Li}_2\text{Na}_2\text{Ti}_6\text{O}_{14}$  exhibits lower electrochemical polarization, quicker kinetic behavior and improved lithium storage capability compared to bare  $\text{Li}_2\text{Na}_2\text{Ti}_6\text{O}_{14}$ . However, few investigations have been reported to enhance the electrochemical performance of  $\text{Li}_2\text{Na}_2\text{Ti}_6\text{O}_{14}$  by doping [20].

In this paper, five Na substituted  $\text{Li}_{2-x}\text{Na}_{2+x}\text{Ti}_6\text{O}_{14}$  (x=0, 0.05, 0.10, 0.15, 0.20) samples are synthesized by a simple solid-state method. The structure, morphology and electrochemical properties of as-prepared sample are described and compared by using various analytical methods. An investigation is carried out to give new insights of Na doping into the evolutions of structural property, ion diffusion, rate performance, charge-discharge behavior of  $\text{Li}_2\text{Na}_2\text{Ti}_6\text{O}_{14}$ .

## 2. Experimental

## 2.1 Sample preparation

In the sample preparation procedure, all the chemical reagents are of analytical grade. Via a simple solid-state method,  $\text{Li}_{2-x}\text{Na}_{2+x}\text{Ti}_6\text{O}_{14}$  ( $x=0, 0.05, 0.10, 0.15, 0.20$ ) samples are prepared using stoichiometric amount of  $\text{CH}_3\text{COOLi}\cdot 2\text{H}_2\text{O}$  (99.0 %),  $\text{CH}_3\text{COONa}\cdot 3\text{H}_2\text{O}$  (99 %) and anatase  $\text{TiO}_2$  (5-10 nm, 99.8 %). The starting materials are mixed by planetary ball milling for 15 hours in ethanol to obtain homogeneous slurry. The resulting slurry is dried at 80 °C for 24 hours, and then calcined at 800 °C for 10 hours in air atmosphere to obtain the final  $\text{Li}_{2-x}\text{Na}_{2+x}\text{Ti}_6\text{O}_{14}$  samples.

## 2.2 Material characterization

The phase identifications are performed on a Bruker D8 Focus X-ray diffractometer with nickel-filtered  $\text{Cu K}\alpha$  radiation ( $\lambda=1.5418 \text{ \AA}$ ), operating at 40 kV and 40 mA. In situ X-ray diffraction (XRD) patterns are collected by the same instrument. The samples are scanned between 5 to 80° ( $2\theta$  degree) using a scan speed of  $0.2^\circ \text{ min}^{-1}$ . The surface morphologies of  $\text{Li}_{2-x}\text{Na}_{2+x}\text{Ti}_6\text{O}_{14}$  samples are observed by a L30 S-FEG field emission scanning electron microscope (SEM), conducting at 10 kV.

## 2.3 Electrode preparation and battery assembly

The working electrodes are prepared by dispersing a mixture of as-prepared active material, carbon black and polyvinylidene fluoride with a weight ratio of 8:1:1 in N-methyl-2-pyrrolidinone to form homogeneous slurry. After mixing, the slurry is pasted on copper foil evenly and then the film is dried at 120 °C in a vacuum oven for 12 hours, followed by cutting into sheets with a diameter of 15 mm. The

two-electrode coin-type cells are assembled in an Ar-filled glove box by using  $\text{Li}_{2-x}\text{Na}_{2+x}\text{Ti}_6\text{O}_{14}$  ( $0 \leq x \leq 0.2$ ) film as working electrode, lithium metal foil as counter electrode, Whatman glass fiber as separator and  $1 \text{ mol L}^{-1}$   $\text{LiPF}_6$  in a 1:1 (v/v) mixture of ethylene carbonate and dimethyl carbonate as electrolyte.

#### 2.4 Electrochemical evaluation

Galvanostatic charge-discharge tests are conducted on Land CT2001A multiple battery test system at a current density of  $100 \text{ mA g}^{-1}$  between 0.0 and 3.0 V. Cyclic voltammograms (CVs) are performed via a computer-controlled CHI 660D electrochemical workstation at a scan rate of  $0.1 \text{ mV s}^{-1}$  between 0.0 and 3.0 V. Electrochemical impedance spectroscopy (EIS) analysis is carried out by CHI 660D electrochemical workstation with an oscillating potential of 5 mV in the frequency ranging from  $10^5$  to  $10^{-2}$  Hz. The cells for EIS observation are three-electrode system with metal lithium foils as reference and counter electrodes. All the tests are carried out at room temperature.

### 3. Results and discussion

Fig. 1 presents the XRD patterns of as-prepared  $\text{Li}_{2-x}\text{Na}_{2+x}\text{Ti}_6\text{O}_{14}$  ( $0 \leq x \leq 0.20$ ) obtained at a temperature of  $800 \text{ }^\circ\text{C}$ . All these patterns are collected on Bruker D8 Focus X-ray diffraction instrument at a room temperature. It can be observed from the XRD curves that the diffraction peak positions and the relative intensities of the prepared samples are well matched with the standard powder diffraction file of JCPDS card No. 52-0690, and it is clear that the diffraction patterns of all samples are

similar with each other. Here, a twin peak appears at 65 °C in Fig. 1 corresponding to (824) and (040) peaks. It also shows from the graph that no impurities are observed in  $\text{Li}_2\text{Na}_2\text{Ti}_6\text{O}_{14}$  and Na doped  $\text{Li}_2\text{Na}_2\text{Ti}_6\text{O}_{14}$  samples. All the results obtained from the above means that the low content Na doping ( $0 \leq x \leq 0.2$ ) does not change the main crystal structure of  $\text{Li}_2\text{Na}_2\text{Ti}_6\text{O}_{14}$ . For a clear observation, the peak position variation of (024) plane is enlarged and shown in Fig. 1b. The compounds with Na doping content of  $x=0.05$  and  $0.10$  exhibit no variation of the diffraction peak, revealing that low Na doping does not affect the lattice parameter of  $\text{Li}_2\text{Na}_2\text{Ti}_6\text{O}_{14}$ . However, the Bragg positions of the Na-doping  $\text{Li}_{2-x}\text{Na}_{2+x}\text{Ti}_6\text{O}_{14}$  samples with  $x=0.15, 0.20$  slightly shift to lower diffraction angles based on the enlarged (024) peak in Fig. 1b, indicating the lattice parameter of  $\text{Li}_{2-x}\text{Na}_{2+x}\text{Ti}_6\text{O}_{14}$  gradually increases after Na doping. The increased lattice parameter should be ascribed to the larger  $\text{Na}^+$  (0.97 Å) replacement of the smaller  $\text{Li}^+$  (0.68 Å) in the sites.

Fig. 2 provides the typical SEM photographs of  $\text{Li}_{2-x}\text{Na}_{2+x}\text{Ti}_6\text{O}_{14}$  ( $0 \leq x \leq 0.20$ ) samples. It is apparent that all the five prepared samples are similar with each other, having a relative uniform morphology with narrow size distribution between 150 and 300 nm. It also can be found that the size of  $\text{Li}_2\text{Na}_2\text{Ti}_6\text{O}_{14}$  is relatively smaller than another four samples, which may attribute to the bigger  $\text{Na}^+$  replacement of the smaller  $\text{Li}^+$  in the structure.

The CV curves of  $\text{Li}_{2-x}\text{Na}_{2+x}\text{Ti}_6\text{O}_{14}$  ( $0 \leq x \leq 0.20$ ) are presented in Fig. 3. All the tests are conducted at room temperature under a scan rate of  $0.1 \text{ mV s}^{-1}$  between 0.0 and 3.0 V. As is shown in Fig. 3a-3e, a pair of characteristic redox peaks can be

observed at around 1.17 and 1.19 V for five samples, regarded as the signature of two lithium-ion per formula insertion into and extraction from the  $\text{Li}_{2-x}\text{Na}_{2+x}\text{Ti}_6\text{O}_{14}$  ( $0 \leq x \leq 0.20$ ) framework [14, 16], which is in consistence with the charge-discharge potential plateaus in Fig. 4. According to the formula of  $\text{Li}_{2-x}\text{Na}_{2+x}\text{Ti}_6\text{O}_{14}$ , a total of six  $\text{Ti}^{4+}$  can be reduced to  $\text{Ti}^{3+}$  after a theoretical evaluation. Thus, the broad peak around 0.0-0.1 V is associated with another four lithium-ion formula storage in the compound. And all the CV peaks are narrow and sharp, corresponding to the rapid kinetic process for lithium ions transportation in the lattices. Besides, pristine  $\text{Li}_2\text{Na}_2\text{Ti}_6\text{O}_{14}$  and  $\text{Li}_{1.95}\text{Na}_{2.05}\text{Ti}_6\text{O}_{14}$  exhibit much obvious reduction peaks at 1.178 V and 1.205, respectively, and a sharper oxidation peaks at 1.362 V than other  $\text{Li}_{2-x}\text{Na}_{2+x}\text{Ti}_6\text{O}_{14}$  ( $0.10 \leq x \leq 0.20$ ) samples. The peak current reduces relatively rapid along with the increase of Na doping concentration from 0.05 to 0.20, revealing a drop in the electrode kinetics. Moreover, the initial three CV curves of  $\text{Li}_2\text{Na}_2\text{Ti}_6\text{O}_{14}$  and  $\text{Li}_{1.95}\text{Na}_{2.05}\text{Ti}_6\text{O}_{14}$  coincide with each other and show higher peak current than the other three ones, indicates that  $\text{Li}_2\text{Na}_2\text{Ti}_6\text{O}_{14}$  and  $\text{Li}_{1.95}\text{Na}_{2.05}\text{Ti}_6\text{O}_{14}$  have higher electrochemical reaction activity and reversibility. The difference between anodic and cathodic peaks can be mainly attributed to the slow lithium ion diffusivity in solid-state body of bulk  $\text{Li}_{2-x}\text{Na}_{2+x}\text{Ti}_6\text{O}_{14}$  ( $0.10 \leq x \leq 0.20$ ) [13]. The potential difference ( $\Delta\phi_p$ ) of  $\text{Li}_{2-x}\text{Na}_{2+x}\text{Ti}_6\text{O}_{14}$  ( $0 \leq x \leq 0.20$ ) electrodes between oxidation and reduction peaks is listed in Table 1. It is obvious that the potential separation ( $\Delta\phi_p$  value) of pristine  $\text{Li}_2\text{Na}_2\text{Ti}_6\text{O}_{14}$  (about 1.82 mV) is much larger than those of Na-doped samples. It suggests that Na doping is beneficial to the reversible

intercalation and deintercalation of  $\text{Li}^+$  in the structure, and then enhances the reversibility of  $\text{Li}_2\text{Na}_2\text{Ti}_6\text{O}_{14}$ . Furthermore,  $\text{Li}_{1.95}\text{Na}_{2.05}\text{Ti}_6\text{O}_{14}$  expresses the smallest potential separation among all the materials, indicating that  $\text{Li}_{1.95}\text{Na}_{2.05}\text{Ti}_6\text{O}_{14}$  may own the best electrochemical performance for its fast electron transfer kinetics and outstanding cycling reversibility.

Fig. 4 depicts the charge and discharge curves upon the 1<sup>st</sup>, 10<sup>th</sup>, 20<sup>th</sup> and 50<sup>th</sup> cycles of  $\text{Li}_{2-x}\text{Na}_{2+x}\text{Ti}_6\text{O}_{14}$  ( $0 \leq x \leq 0.20$ ) samples at the potential range of 0.0-3.0 V. As is shown in Fig. 4a, all above-mentioned compounds exhibit one charge plateau and one discharge plateau, similar to the previous report of  $\text{Li}_2\text{Na}_2\text{Ti}_6\text{O}_{14}$  [14-17]. For the initial cycle of  $\text{Li}_{2-x}\text{Na}_{2+x}\text{Ti}_6\text{O}_{14}$  ( $0 \leq x \leq 0.20$ ), the potential drops rapidly from open-circuit potential to 1.35 V, and then the discharge potential maintains for a long flat platform at a average potential of 1.24 V. Finally, a long slope appears between 0.0 and 1.2 V. During the charging process, the charge plateaus of  $\text{Li}_{2-x}\text{Na}_{2+x}\text{Ti}_6\text{O}_{14}$  ( $x=0.00, 0.10, 0.15$  and  $0.20$ ) are at about 1.34 V. In contrast, the plateau of  $\text{Li}_{1.95}\text{Na}_{2.05}\text{Ti}_6\text{O}_{14}$  keeps nearly at 1.30 V, and then rapidly increases to the cut-off potential. It reveals that  $\text{Li}_{1.95}\text{Na}_{2.05}\text{Ti}_6\text{O}_{14}$  has lower charge/discharge polarization (0.05 V) than that (0.11 V) of  $\text{Li}_{2-x}\text{Na}_{2+x}\text{Ti}_6\text{O}_{14}$  ( $x=0.00, 0.10, 0.15, 0.20$ ), which is also in correspondence with the results of CV curves. Besides, it is evident that the charge plateau of  $\text{Li}_{1.95}\text{Na}_{2.05}\text{Ti}_6\text{O}_{14}$  are much longer than those of  $\text{Li}_{2-x}\text{Na}_{2+x}\text{Ti}_6\text{O}_{14}$  ( $x=0.00, 0.10, 0.15, 0.20$ ) in all of four graphs. After 50 cycles,  $\text{Li}_{1.95}\text{Na}_{2.05}\text{Ti}_6\text{O}_{14}$  still exhibits the discharge and charge plateaus at around 1.16 and 1.33 V, respectively. Its charge-discharge polarization remains much lower than those of  $\text{Li}_{2-x}\text{Na}_{2+x}\text{Ti}_6\text{O}_{14}$

( $x=0.00, 0.10, 0.15, 0.20$ ), which further confirm the superior cycling performance of  $\text{Li}_{1.95}\text{Na}_{2.05}\text{Ti}_6\text{O}_{14}$ .

To further conduct investigation of the electrochemical properties for  $\text{Li}_{2-x}\text{Na}_{2+x}\text{Ti}_6\text{O}_{14}$  ( $0 \leq x \leq 0.20$ ), the cycling performance and corresponding cycling coulombic efficiencies upon repeated cycles are also shown in Fig. 5. It can be clearly observed that  $\text{Li}_{1.95}\text{Na}_{2.05}\text{Ti}_6\text{O}_{14}$  express the highest charge capacity of  $243.6 \text{ mAh g}^{-1}$  for the first cycle, while  $\text{Li}_2\text{Na}_2\text{Ti}_6\text{O}_{14}$ ,  $\text{Li}_{1.9}\text{Na}_{2.1}\text{Ti}_6\text{O}_{14}$ ,  $\text{Li}_{1.85}\text{Na}_{2.15}\text{Ti}_6\text{O}_{14}$  and  $\text{Li}_{1.8}\text{Na}_{2.2}\text{Ti}_6\text{O}_{14}$  only deliver the initial charge capacity of 240.1, 229.0, 214.0 and 225.2  $\text{mAh g}^{-1}$ , respectively. Besides,  $\text{Li}_{1.95}\text{Na}_{2.05}\text{Ti}_6\text{O}_{14}$  still remains the charge capacity of  $210.7 \text{ mAh g}^{-1}$  after 79 repeated cycles, which proves that appropriate amount Na doping is beneficial to improve the cycling stability of  $\text{Li}_2\text{Na}_2\text{Ti}_6\text{O}_{14}$ . On the other hand,  $\text{Li}_2\text{Na}_2\text{Ti}_6\text{O}_{14}$ ,  $\text{Li}_{1.9}\text{Na}_{2.1}\text{Ti}_6\text{O}_{14}$ ,  $\text{Li}_{1.85}\text{Na}_{2.15}\text{Ti}_6\text{O}_{14}$  and  $\text{Li}_{1.8}\text{Na}_{2.2}\text{Ti}_6\text{O}_{14}$  only hold the reversible capacity of 159.1, 203.5, 190.1 and 156.7  $\text{mAh g}^{-1}$ , respectively, implying high Na doping content goes against the cycling performance. Therefore, it is known that the superior cycling performance of  $\text{Li}_{1.95}\text{Na}_{2.05}\text{Ti}_6\text{O}_{14}$  is attributed to the low content Na doping in the structure, which may improve the lithium ion diffusivity and structural stability of  $\text{Li}_2\text{Na}_2\text{Ti}_6\text{O}_{14}$ . Furthermore, the corresponding cycling coulombic efficiencies upon repeated cycles are shown in Fig. 5b. Among the five compounds,  $\text{Li}_{1.95}\text{Na}_{2.05}\text{Ti}_6\text{O}_{14}$  still presents the highest average cycling efficiency of 99.0 %, while the others hold the cycling coulombic efficiency of nearly 94.5-98.0 %, which further indicates the outstanding cycling performance of  $\text{Li}_{1.95}\text{Na}_{2.05}\text{Ti}_6\text{O}_{14}$ .

Fig. 6a displays the Nyquist plots before cycles for the as-prepared  $\text{Li}_{2-x}\text{Na}_{2+x}\text{Ti}_6\text{O}_{14}$  ( $0 \leq x \leq 0.20$ ). The enlarged Nyquist curves of  $\text{Li}_{2-x}\text{Na}_{2+x}\text{Ti}_6\text{O}_{14}$  ( $0 \leq x \leq 0.20$ ) in the high frequency region are also shown in Fig. 6a as an insert graph. All the curves have one semi-circle in the high-frequency region and a straight line in low-frequency region, which are related with the charge transfer process and lithium ion diffusion behavior. The EIS patterns can be used to calculate the lithium diffusion coefficient ( $D_{\text{Li}}$ ), which is an important factor to evaluate the electrochemical kinetics of compounds. Here, the  $D_{\text{Li}}$  of lithium ion can be calculated by the following equation [4, 21]:

$$D_{\text{Li}} = \frac{(RT)^2}{2(A n^2 F^2 C_{\text{Li}} \sigma)^2} \quad (1)$$

Where  $R$  is the gas constant ( $8.314 \text{ J mol}^{-1} \text{ K}^{-1}$ ),  $T$  is the absolute temperature for battery testing (298 K),  $A$  is the surface area of electrode ( $1.766 \text{ cm}^2$ ),  $n$  is the number of electrons transfer during the electrochemical reaction,  $F$  is the Faraday constant ( $94850 \text{ C mol}^{-1}$ ),  $C_{\text{Li}}$  is the concentration of lithium ion in the compound, and the Warburg factor  $\sigma$  can be calculated from the plots in the low-frequency region, and the relationship of  $\sigma$  with  $Z_{\text{re}}$  is as follows:

$$Z_{\text{re}} = R_{\text{ct}} + R_s + \sigma \omega^{\frac{1}{2}} \quad (2)$$

The  $Z_{\text{re}}-\sigma$  plots are shown in Fig. 6b, and a linear characteristic could be seen from the curves. Based on the equations (1) and (2), the calculated diffusion coefficients are listed in Table 2. Observed from Table 2, it is clear that  $\text{Li}_{1.95}\text{Na}_{2.05}\text{Ti}_6\text{O}_{14}$  possesses the highest lithium ion diffusion coefficient of  $1.11 \times 10^{-14} \text{ cm}^2 \text{ s}^{-1}$ , while the pristine  $\text{Li}_2\text{Na}_2\text{Ti}_6\text{O}_{14}$  only reveals a low lithium ion diffusion

coefficient of  $1.57 \times 10^{-15} \text{ cm}^2 \text{ s}^{-1}$ . With the increase of Na doping content, the lithium ion diffusion coefficient finally reduces to  $4.37 \times 10^{-15} \text{ cm}^2 \text{ s}^{-1}$  with  $x=2.0$  in  $\text{Li}_{2-x}\text{Na}_{2+x}\text{Ti}_6\text{O}_{14}$ . It suggests that appropriate amount Na doping is beneficial to improve the lithium ion diffusivity and kinetic behavior of  $\text{Li}_2\text{Na}_2\text{Ti}_6\text{O}_{14}$ . Therefore, it is expected that  $\text{Li}_{1.95}\text{Na}_{2.05}\text{Ti}_6\text{O}_{14}$  may have an outstanding rate property.

Fig. 7 delivers the initial charge-discharge curves of  $\text{Li}_{2-x}\text{Na}_{2+x}\text{Ti}_6\text{O}_{14}$  ( $0 \leq x \leq 0.20$ ) samples at 200, 300 and 400  $\text{mA g}^{-1}$ . It can be found that  $\text{Li}_2\text{Na}_2\text{Ti}_6\text{O}_{14}$ ,  $\text{Li}_{1.95}\text{Na}_{2.05}\text{Ti}_6\text{O}_{14}$  and  $\text{Li}_{1.9}\text{Na}_{2.1}\text{Ti}_6\text{O}_{14}$  show a flat plateau at around 1.34 V for the charge plot and a flat plateau at about 1.20 V for the discharge plot. In contrast,  $\text{Li}_{1.85}\text{Na}_{2.15}\text{Ti}_6\text{O}_{14}$  and  $\text{Li}_{1.8}\text{Na}_{2.2}\text{Ti}_6\text{O}_{14}$  display the discharge and charge plateaus at 0.98 and 1.48 V, respectively. The results indicate that  $\text{Li}_2\text{Na}_2\text{Ti}_6\text{O}_{14}$ ,  $\text{Li}_{1.95}\text{Na}_{2.05}\text{Ti}_6\text{O}_{14}$  and  $\text{Li}_{1.9}\text{Na}_{2.1}\text{Ti}_6\text{O}_{14}$  maintain lower electrochemical polarization than  $\text{Li}_{1.85}\text{Na}_{2.15}\text{Ti}_6\text{O}_{14}$  and  $\text{Li}_{1.8}\text{Na}_{2.2}\text{Ti}_6\text{O}_{14}$  during high rate discharge-charge cycles, even at a current density of 400  $\text{mA g}^{-1}$ . It also suggests that  $\text{Li}_2\text{Na}_2\text{Ti}_6\text{O}_{14}$ ,  $\text{Li}_{1.95}\text{Na}_{2.05}\text{Ti}_6\text{O}_{14}$  and  $\text{Li}_{1.9}\text{Na}_{2.1}\text{Ti}_6\text{O}_{14}$  may have better kinetic properties at high rates.

The rate performances of five  $\text{Li}_{2-x}\text{Na}_{2+x}\text{Ti}_6\text{O}_{14}$  ( $0 \leq x \leq 0.20$ ) samples are presented in Fig. 8. Extended galvanostatic cycles of the  $\text{Li}_{2-x}\text{Na}_{2+x}\text{Ti}_6\text{O}_{14}$  electrodes are performed at increasing current density of 150, 200, 250, 300, 350 and 400  $\text{mA g}^{-1}$ . Viewed from Fig. 8, it is obvious that the pristine  $\text{Li}_2\text{Na}_2\text{Ti}_6\text{O}_{14}$  only maintains the lithium storage capacity of 206.5  $\text{mAh g}^{-1}$  at 200  $\text{mA g}^{-1}$ , 194.6  $\text{mAh g}^{-1}$  at 300  $\text{mA g}^{-1}$ , and 186.6  $\text{mAh g}^{-1}$  at 400  $\text{mA g}^{-1}$ . With the increase of Na doping content, the rate performance of  $\text{Li}_{2-x}\text{Na}_{2+x}\text{Ti}_6\text{O}_{14}$  shows an improvement at low Na content and then

presents a decrease at high Na content. Compared with other four samples,  $\text{Li}_{1.95}\text{Na}_{2.05}\text{Ti}_6\text{O}_{14}$  apparently delivers a better performance with the charge capacity of  $221.1 \text{ mAh g}^{-1}$  at  $200 \text{ mA g}^{-1}$ ,  $211.9 \text{ mAh g}^{-1}$  at  $300 \text{ mA g}^{-1}$ , and  $198.7 \text{ mAh g}^{-1}$  at  $400 \text{ mA g}^{-1}$ . This result is roughly consistent with the cycling performance as shown in Fig. 5a. From what have discussed above, it can be concluded that the incorporation of low sodium content  $x=0.05$  provokes positive effect on ionic conductivity and the electrochemical properties for  $\text{Li}_2\text{Na}_2\text{Ti}_6\text{O}_{14}$ .

To observe the structural evolution of Na-doped  $\text{Li}_2\text{Na}_2\text{Ti}_6\text{O}_{14}$ , in situ XRD technique is used to investigate the reversibility of  $\text{Li}_{1.95}\text{Na}_{2.05}\text{Ti}_6\text{O}_{14}$ . The description of in situ cell and its preparation process can be found in our previous paper [22]. Fig. 9-11 shows that the characteristic diffraction peaks of  $\text{Li}_{1.95}\text{Na}_{2.05}\text{Ti}_6\text{O}_{14}$  gradually shift to lower Bragg positions during the lithiation process. With a reverse delithiation reaction, all the featured peaks can go back the original positions. It suggests that the structural change of  $\text{Li}_{1.95}\text{Na}_{2.05}\text{Ti}_6\text{O}_{14}$  is highly reversible during the charge/discharge process. As a result, the stable host structure of  $\text{Li}_{1.95}\text{Na}_{2.05}\text{Ti}_6\text{O}_{14}$  can ensure the long-term repeated electrochemical cycles.

#### 4. Conclusions

Via Li-site substitution with Na, five  $\text{Li}_{2-x}\text{Na}_{2+x}\text{Ti}_6\text{O}_{14}$  ( $0 \leq x \leq 0.20$ ) samples are prepared by a simple solid-state method. XRD results reveal that all the as-prepared samples are single-phase without any impurity. Morphological characterization shows that all the five samples are well-crystallized products with a homogeneous particle

size between 150 and 300 nm. Electrochemical analysis shows that  $\text{Li}_{1.95}\text{Na}_{2.05}\text{Ti}_6\text{O}_{14}$  exhibits the highest reversible capacity and the best rate property among all the  $\text{Li}_2\text{Na}_2\text{Ti}_6\text{O}_{14}$ -type anodes. Compared with other four samples,  $\text{Li}_{1.95}\text{Na}_{2.05}\text{Ti}_6\text{O}_{14}$  can deliver a better rate performance with the charge capacity of  $221.1 \text{ mAh g}^{-1}$  at  $200 \text{ mA g}^{-1}$ ,  $211.9 \text{ mAh g}^{-1}$  at  $300 \text{ mA g}^{-1}$ , and  $198.7 \text{ mAh g}^{-1}$  at  $400 \text{ mA g}^{-1}$ . EIS results prove that the improved lithium storage performance of Na-doped  $\text{Li}_2\text{Na}_2\text{Ti}_6\text{O}_{14}$  is related to the improved ionic conductivity and the decreased redox polarization via Li-site substitution with Na. Besides, the reversible structural change of  $\text{Li}_{1.95}\text{Na}_{2.05}\text{Ti}_6\text{O}_{14}$  as observed by in situ XRD proves its stable host structure for repeated lithium storage.

### Acknowledgements

This work is sponsored by Ningbo Key Innovation Team (2014B81005) and Ningbo Natural Science Foundation (2014A610042). The work is also supported by opening project of Key Laboratory of Photochemical Conversion and Optoelectronic Materials, TIPC, CAS (PCOM201408) and K.C. Wong Magna Fund in Ningbo University.

### References

- [1] J.M. Tarascon, M. Armand, Issues and challenges facing rechargeable lithium batteries, *Nature* 414 (2001) 359-367.
- [2] M. Armand, J.M. Tarascon, Building better batteries, *Nature* 451 (2008) 652-657.

- [3] S.S. Zhang. The effect of the charging protocol on the cycle life of a Li-ion battery, *Journal of Power Sources* 161 (2006) 1385-1391.
- [4] T. Yi, H. Liu, Y. Zhu, L. Jiang, Y. Xie, R. Zhu. Improving the high rate performance of  $\text{Li}_4\text{Ti}_5\text{O}_{12}$  through divalent zinc substitution, *Journal of Power Sources* 215 (2012) 258-265.
- [5] T. Takashima, T. Tojo, R. Inada, Y. Sakurai, Characterization of mixed titanium–niobium oxide  $\text{Ti}_2\text{Nb}_{10}\text{O}_{29}$  annealed in vacuum as anode material for lithium-ion battery, *Journal of Power Sources* 276 (2015) 113-119.
- [6] J. Akimoto, K. Kataoka, N. Kojima, S. Hayashi, Y. Gotoh, T. Sotokawa, Y. Kumashiro, A novel soft-chemical synthetic route using  $\text{Na}_2\text{Ti}_6\text{O}_{13}$  as a starting compound and electrochemical properties of  $\text{H}_2\text{Ti}_{12}\text{O}_{25}$ , *Journal of Power Sources* 244 (2013) 679-683.
- [7] W. Cho, M.S. Park, J.H. Kim, Y.J. Kim, Interfacial reaction between electrode and electrolyte for a ramsdellite type  $\text{Li}_{2+x}\text{Ti}_3\text{O}_7$  anode material during lithium insertion, *Electrochimica Acta* 63 (2012) 263-268.
- [8] J.C. Pérez-Flores, A. Kuhn, F. García-Alvarado, Synthesis, structure and electrochemical Li insertion behaviour of  $\text{Li}_2\text{Ti}_6\text{O}_{13}$  with the  $\text{Na}_2\text{Ti}_6\text{O}_{13}$  tunnel-structure, *Journal of Power Sources* 196 (2011) 1378-1385.
- [9] J. Liu, Y. Li, X. Wang, Y. Gao, N. Wu, B. Wu Synthesis process investigation and electrochemical performance characterization of  $\text{SrLi}_2\text{Ti}_6\text{O}_{14}$  by ex situ XRD, *Journal of Alloys and Compounds* 581 (2013) 236-240.

- [10] D. Dambournet, I. Belharouak, J. Ma, K. Amine, Template-assisted synthesis of high packing density  $\text{SrLi}_2\text{Ti}_6\text{O}_{14}$  for use as anode in 2.7-V lithium-ion battery, *Journal of Power Sources* 196 (2011) 2871-2874.
- [11] J. Liu, X. Sun, Y. Li, X. Wang, Y. Gao, K. Wu, N. Wu, B. Wu, Electrochemical performance of  $\text{LiCoO}_2/\text{SrLi}_2\text{Ti}_6\text{O}_{14}$  batteries for high-power applications, *Journal of Power Sources* 245 (2014) 371-376.
- [12] I. Koseva, J.P. Chaminade, P. Gravereau, S. Pechev, P. Peshev, J. Etourneau, A new family of isostructural titanates,  $\text{MLi}_2\text{Ti}_6\text{O}_{14}$  (M = Sr, Ba, Pb), *Journal of Alloys and Compounds* 389 (2005) 47-54.
- [13] X.T. Lin, P. Li, L.Y. Shao, M. Shui, D.J. Wang, N.B. Long, Y.L. Ren, J. Shu, Lithium barium titanate: A stable lithium storage material for lithium-ion batteries, *Journal of Power Sources* 278 (2015) 546-554.
- [14] D. Dambournet, I. Belharouak, K. Amine,  $\text{MLi}_2\text{Ti}_6\text{O}_{14}$  (M = Sr, Ba, 2Na) lithium insertion titanate materials: A comparative study, *Inorganic Chemistry* 49 (2010) 2822-2826.
- [15] S.Y. Yin, L. Song, X.Y. Wang, Y.H. Huang, K.L. Zhang, Y.X. Zhang. Reversible lithium storage in  $\text{Na}_2\text{Li}_2\text{Ti}_6\text{O}_{14}$  as anode for lithium ion batteries, *Electrochemistry Communications* 11 (2009) 1251-1254.
- [16] K. Wu, D. Wang, X. Lin, L. Shao, M. Shui, X. Jiang, N. Long, Y. Ren, J. Shu. Comparative study of  $\text{Na}_2\text{Li}_2\text{Ti}_6\text{O}_{14}$  prepared by different methods as advanced anode material for lithium-ion batteries, *Journal of Electroanalytical Chemistry* 717-718 (2014) 10-16.

- [17] K. Wu, J. Shu, X. Lin, L. Shao, M. Lao, M. Shui, P. Li, N. Long, D. Wang, Enhanced electrochemical performance of sodium lithium titanate by coating various carbons, *Journal of Power Sources* 272 (2014) 283-290.
- [18] K. Wu, X. Lin, L. Shao, M. Shui, N. Long, Y. Ren, J. Shu. Copper/carbon coated lithium sodium titanate as advanced anode material for lithium-ion batteries, *Journal of Power Sources* 259 (2014) 177-182.
- [19] K. Wu, J. Shu, X. Lin, L. Shao, P. Li, M. Shui, M. Lao, N. Long, D. Wang, Phase composition and electrochemical performance of sodium lithium titanates as anode materials for lithium rechargeable batteries, *Journal of Power Sources* 275 (2015) 419-428.
- [20] M. Lao, X. Lin, P. Li, L. Shao, K. Wu, M. Shui, N. Long, Y. Ren, J. Shu, Preparation and electrochemical characterization of  $\text{Li}_{2+x}\text{Na}_{2-x}\text{Ti}_6\text{O}_{14}$  ( $0 \leq x \leq 0.2$ ) as anode materials for lithium-ion batteries, *Ceramics International* 41 (2015) 2900-2907.
- [21] T. Yi, S. Yang, X. Li, J. Yao, Y. Zhu, R. Zhu. Sub-micrometric  $\text{Li}_{4-x}\text{Na}_x\text{Ti}_5\text{O}_{12}$  spinel as anode material exhibiting high rate capability, *Journal of Power Sources*, 246 (2014) 505-511.
- [22] J. Shu, M. Shui, D. Xu, Y.L. Ren, D.J. Wang, Q.C. Wang, R. Ma, W.D. Zheng, S. Gao, L. Hou, J.J. Xu, J. Cui, Z.H. Zhu, M. Li, Large-scale synthesis of  $\text{Li}_{1.15}\text{V}_3\text{O}_8$  nanobelts and their lithium storage behavior studied by in situ X-ray diffraction, *Journal of Materials Chemistry* 22 (2012) 3035-3043.

**Figure captions**

**Fig. 1.** XRD patterns of  $\text{Li}_{2-x}\text{Na}_{2+x}\text{Ti}_6\text{O}_{14}$  ( $0 \leq x \leq 0.20$ ) samples. (a) Full patterns, (b) local patterns.

**Fig. 2.** SEM images of  $\text{Li}_{2-x}\text{Na}_{2+x}\text{Ti}_6\text{O}_{14}$  samples. (a, b)  $x=0.00$ , (c, d)  $x=0.05$ , (e, f)  $x=0.10$ , (g, h)  $x=0.15$ , (i, j)  $x=0.20$ .

**Fig. 3.** CVs of  $\text{Li}_{2-x}\text{Na}_{2+x}\text{Ti}_6\text{O}_{14}$  ( $0 \leq x \leq 0.20$ ) samples. (a)  $\text{Li}_2\text{Na}_2\text{Ti}_6\text{O}_{14}$ , (b)  $\text{Li}_{1.95}\text{Na}_{2.05}\text{Ti}_6\text{O}_{14}$ , (c)  $\text{Li}_{1.9}\text{Na}_{2.1}\text{Ti}_6\text{O}_{14}$ , (d)  $\text{Li}_{1.85}\text{Na}_{2.15}\text{Ti}_6\text{O}_{14}$ , (e)  $\text{Li}_{1.8}\text{Na}_{2.2}\text{Ti}_6\text{O}_{14}$ .

**Fig. 4.** The 1<sup>st</sup> (a), 10<sup>th</sup> (b), 20<sup>th</sup> (c) 50<sup>th</sup> (d) and 79<sup>th</sup> (d) charge/discharge curves of  $\text{Li}_{2-x}\text{Na}_{2+x}\text{Ti}_6\text{O}_{14}$  ( $0 \leq x \leq 0.20$ ) samples at a current density of  $100 \text{ mA g}^{-1}$ .

**Fig. 5.** (a) Cycle performance and (b) corresponding coulombic efficiency of  $\text{Li}_{2-x}\text{Na}_{2+x}\text{Ti}_6\text{O}_{14}$  ( $0 \leq x \leq 0.20$ ) samples.

**Fig. 6.** (a) EIS patterns before cycles and (b) corresponding  $Z_{\text{re}}$  vs.  $\omega^{-0.5}$  curves at the low frequency range for  $\text{Li}_{2-x}\text{Na}_{2+x}\text{Ti}_6\text{O}_{14}$  ( $0 \leq x \leq 0.20$ ) samples.

**Fig. 7.** The comparative charge/discharge curves of  $\text{Li}_{2-x}\text{Na}_{2+x}\text{Ti}_6\text{O}_{14}$  ( $0 \leq x \leq 0.20$ ) samples at different current densities. (a)  $200 \text{ mA g}^{-1}$ , (b)  $300 \text{ mA g}^{-1}$ , and (c)  $400 \text{ mA g}^{-1}$ .

**Fig. 8.** Rate performance of  $\text{Li}_{2-x}\text{Na}_{2+x}\text{Ti}_6\text{O}_{14}$  ( $0 \leq x \leq 0.20$ ) samples.

**Fig. 9.** Overall In situ XRD patterns of  $\text{Li}_{1.95}\text{Na}_{2.05}\text{Ti}_6\text{O}_{14}$  during the charge/discharge process.

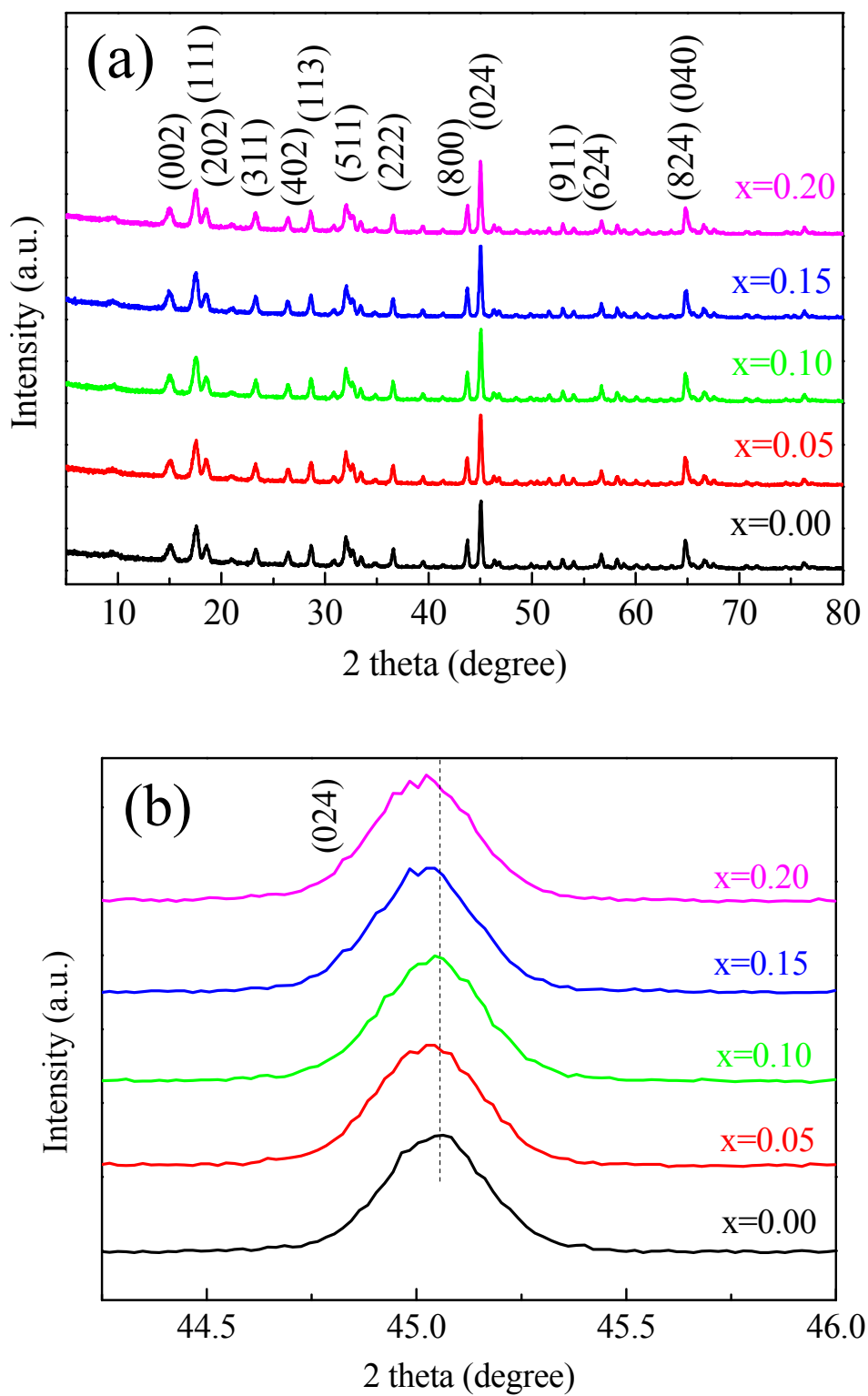
**Fig. 10.** Selected In situ XRD patterns of  $\text{Li}_{1.95}\text{Na}_{2.05}\text{Ti}_6\text{O}_{14}$  with the same background.

**Fig. 11.** The evolution of relative intensity versus Bragg position of  $\text{Li}_{1.95}\text{Na}_{2.05}\text{Ti}_6\text{O}_{14}$  during the charge/discharge process.

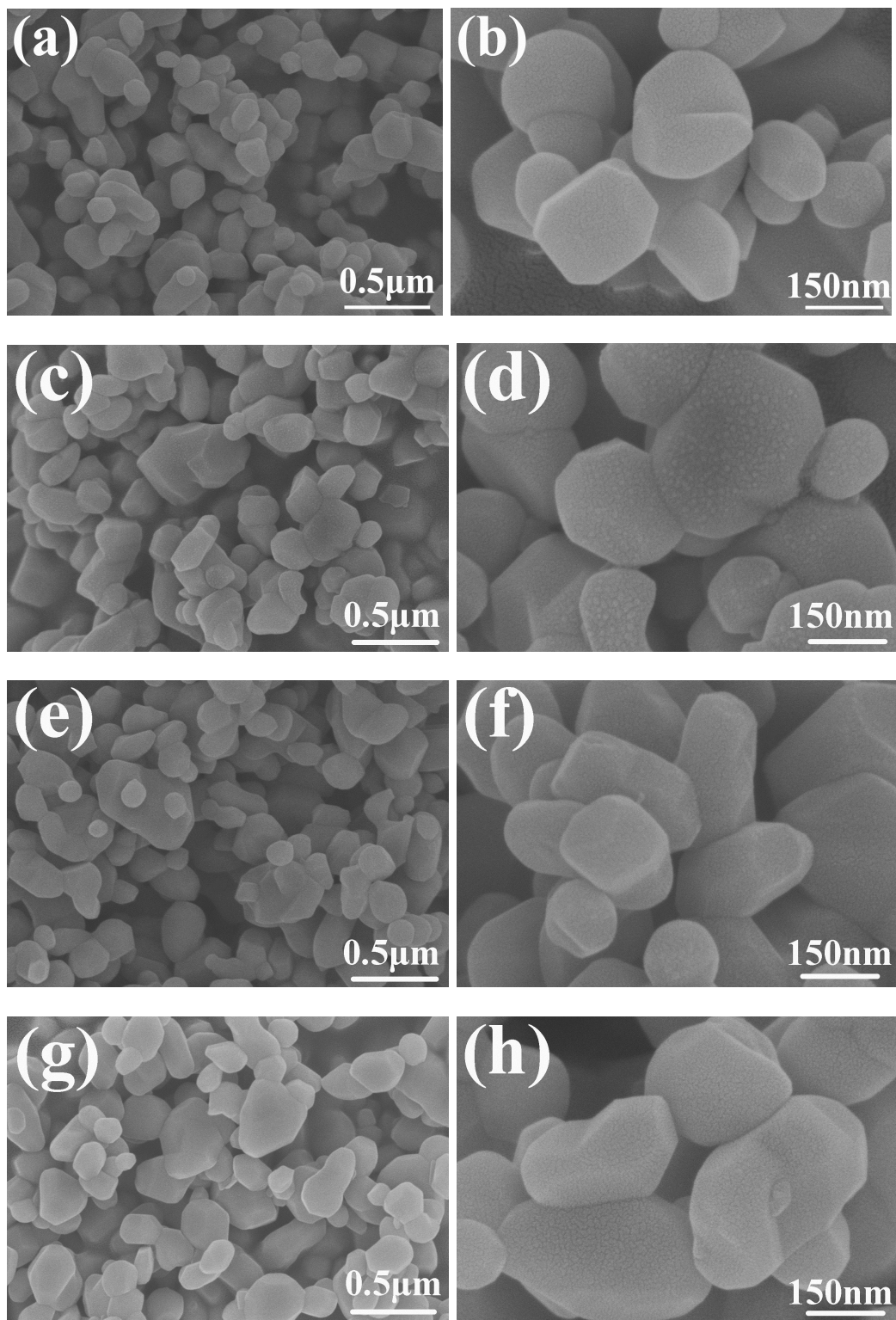
**Table captions**

**Table 1.** Potentials of the redox peaks in the CVs for  $\text{Li}_{2-x}\text{Na}_{2+x}\text{Ti}_6\text{O}_{14}$  ( $0 \leq x \leq 0.20$ ) samples.

**Table 2.** The  $\text{Li}^+$  diffusion coefficients calculated from EIS patterns for  $\text{Li}_{2-x}\text{Na}_{2+x}\text{Ti}_6\text{O}_{14}$  ( $0 \leq x \leq 0.20$ ) samples.



**Fig. 1.** XRD patterns of  $\text{Li}_{2-x}\text{Na}_{2+x}\text{Ti}_6\text{O}_{14}$  ( $0 \leq x \leq 0.20$ ) samples. (a) Full patterns, (b) local patterns.



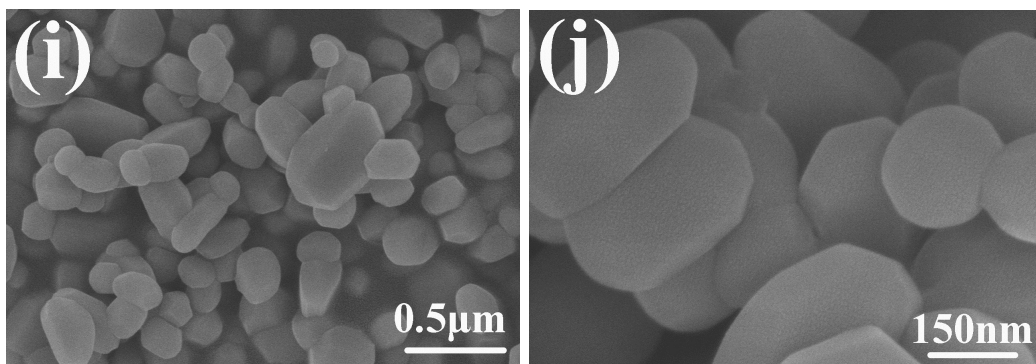


**Fig. 2.** SEM images of  $\text{Li}_{2-x}\text{Na}_{2+x}\text{Ti}_6\text{O}_{14}$  samples. (a, b)  $x=0.00$ , (c, d)  $x=0.05$ , (e, f)  $x=0.10$ , (g, h)  $x=0.15$ , (i, j)  $x=0.20$ .

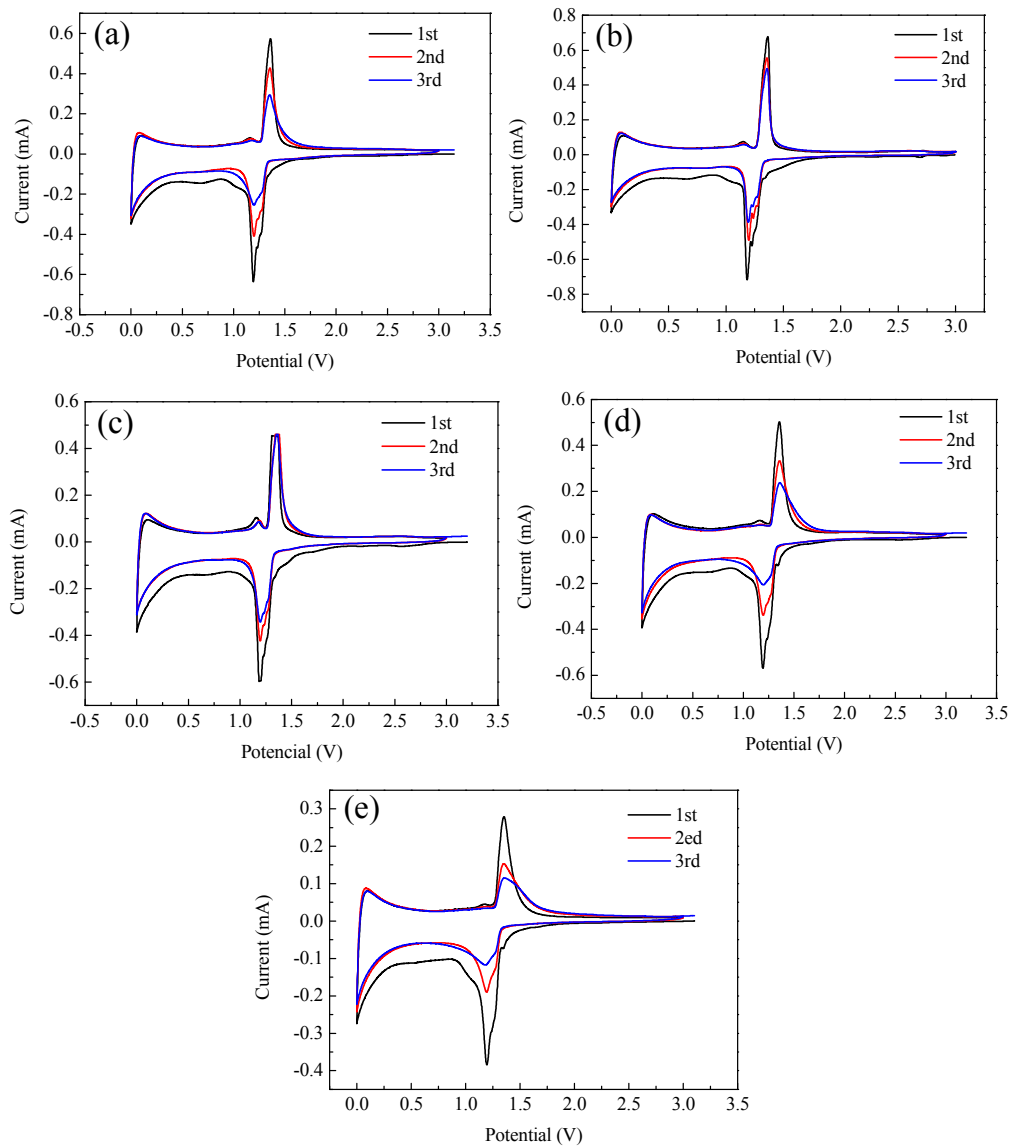


**Fig. 3.** CVs of  $\text{Li}_{2-x}\text{Na}_{2+x}\text{Ti}_6\text{O}_{14}$  ( $0 \leq x \leq 0.20$ ) samples. (a)  $\text{Li}_2\text{Na}_2\text{Ti}_6\text{O}_{14}$ , (b)  $\text{Li}_{1.95}\text{Na}_{2.05}\text{Ti}_6\text{O}_{14}$ , (c)  $\text{Li}_{1.9}\text{Na}_{2.1}\text{Ti}_6\text{O}_{14}$ , (d)  $\text{Li}_{1.85}\text{Na}_{2.15}\text{Ti}_6\text{O}_{14}$ , (e)  $\text{Li}_{1.8}\text{Na}_{2.2}\text{Ti}_6\text{O}_{14}$ .

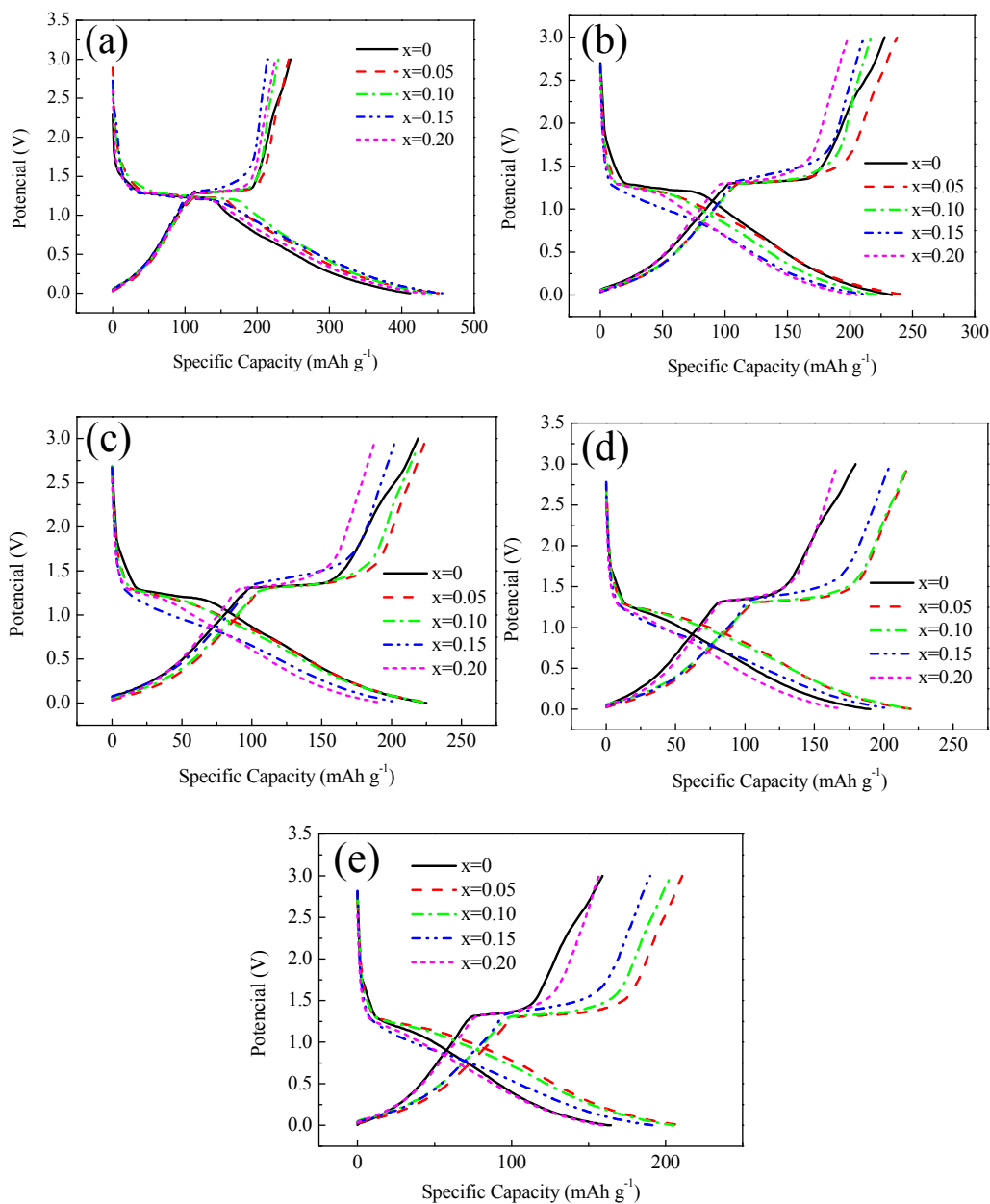


**Fig. 4.** The 1<sup>st</sup> (a), 10<sup>th</sup> (b), 20<sup>th</sup> (c) 50<sup>th</sup> (d) and 79<sup>th</sup> (d) charge/discharge curves of

$\text{Li}_{2-x}\text{Na}_{2+x}\text{Ti}_6\text{O}_{14}$  ( $0 \leq x \leq 0.20$ ) samples at a current density of 100 mA g<sup>-1</sup>.

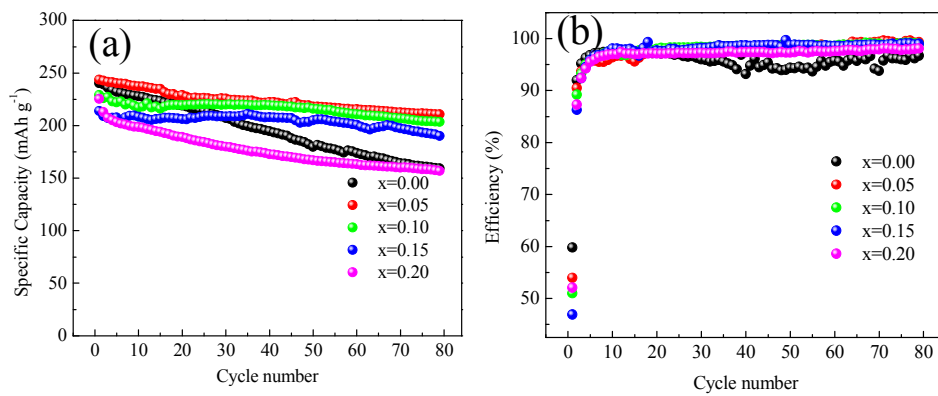


**Fig. 5.** (a) Cycle performance and (b) corresponding coulombic efficiency of

$\text{Li}_{2-x}\text{Na}_{2+x}\text{Ti}_6\text{O}_{14}$  ( $0 \leq x \leq 0.20$ ) samples.

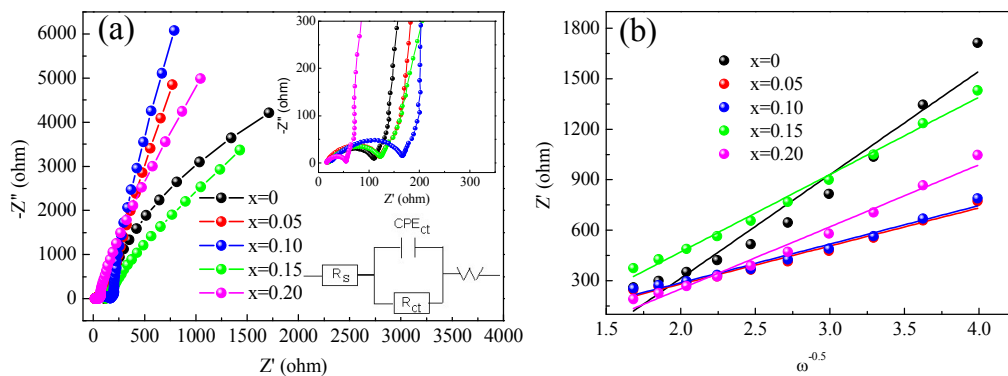


**Fig. 6.** (a) EIS patterns before cycles and (b) corresponding  $Z_{rc}$  vs.  $\omega^{-0.5}$  curves at the low frequency range for  $\text{Li}_{2-x}\text{Na}_{2+x}\text{Ti}_6\text{O}_{14}$  ( $0 \leq x \leq 0.20$ ) samples.

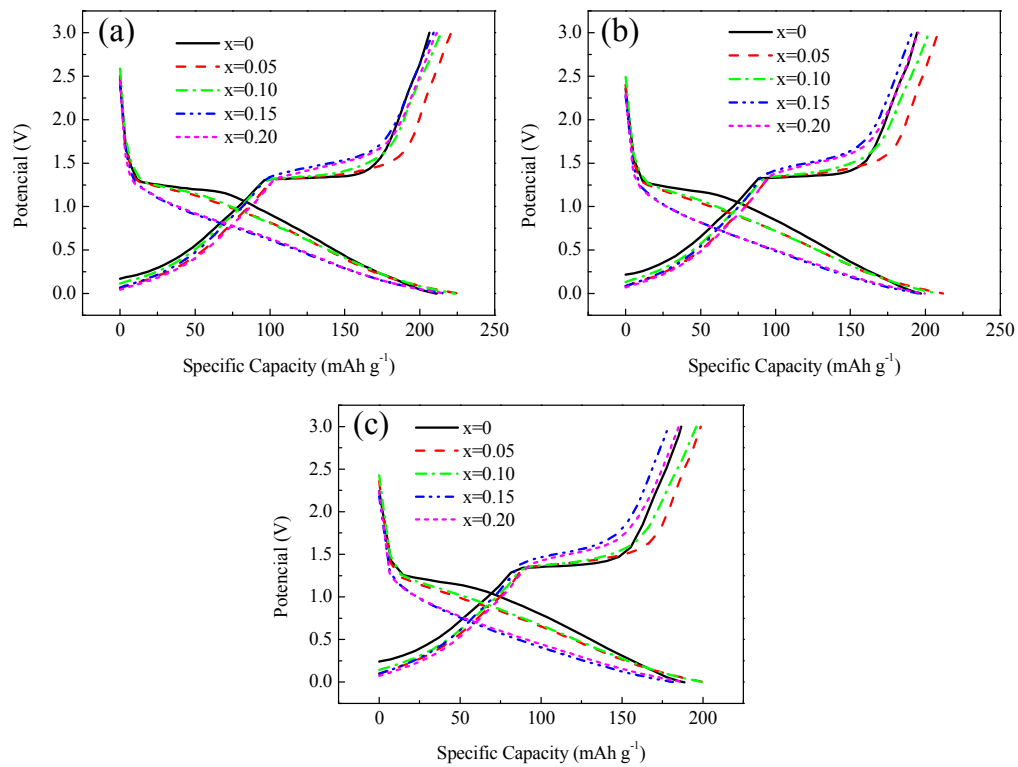


**Fig. 7.** The comparative charge/discharge curves of  $\text{Li}_{2-x}\text{Na}_{2+x}\text{Ti}_6\text{O}_{14}$  ( $0 \leq x \leq 0.20$ ) samples at different current densities. (a)  $200 \text{ mA g}^{-1}$ , (b)  $300 \text{ mA g}^{-1}$ , and (c)  $400 \text{ mA g}^{-1}$ .

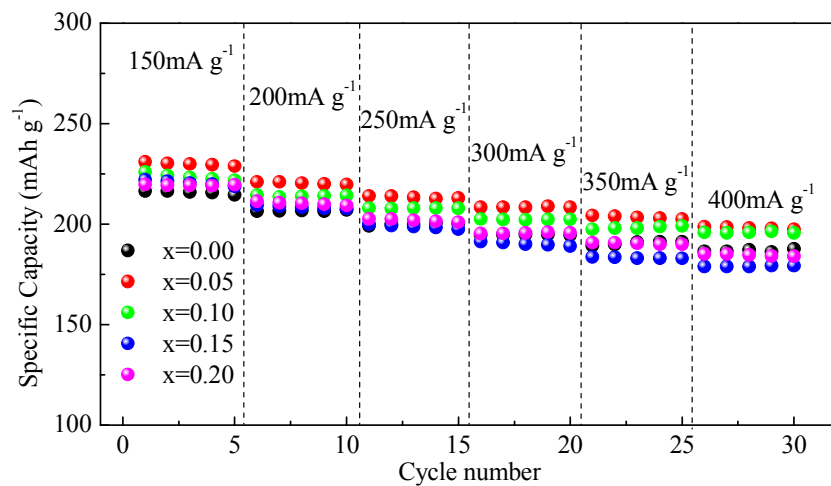


**Fig. 8.** Rate performance of  $\text{Li}_{2-x}\text{Na}_{2+x}\text{Ti}_6\text{O}_{14}$  ( $0 \leq x \leq 0.20$ ) samples.

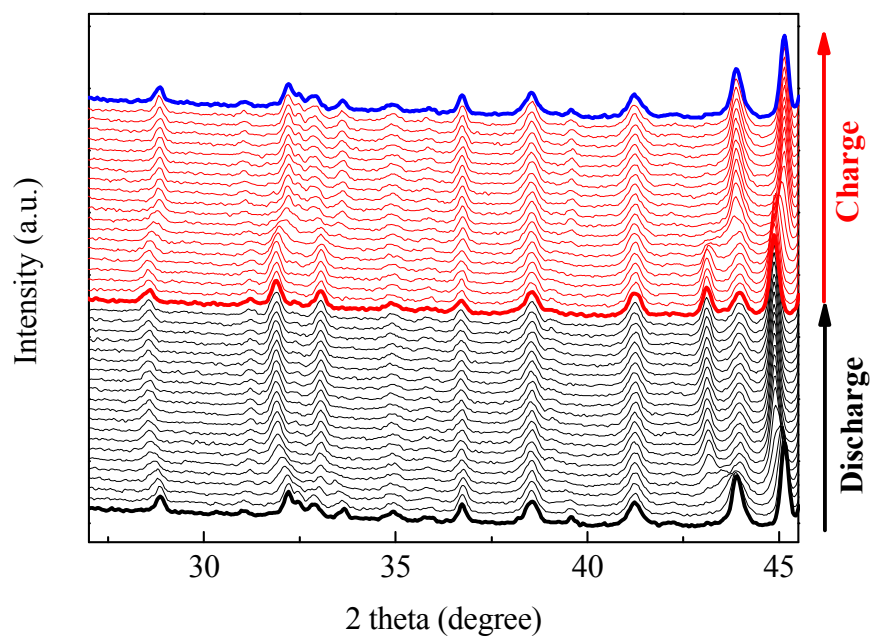


**Fig. 9.** Overall In situ XRD patterns of  $\text{Li}_{1.95}\text{Na}_{2.05}\text{Ti}_6\text{O}_{14}$  during the charge/discharge process.

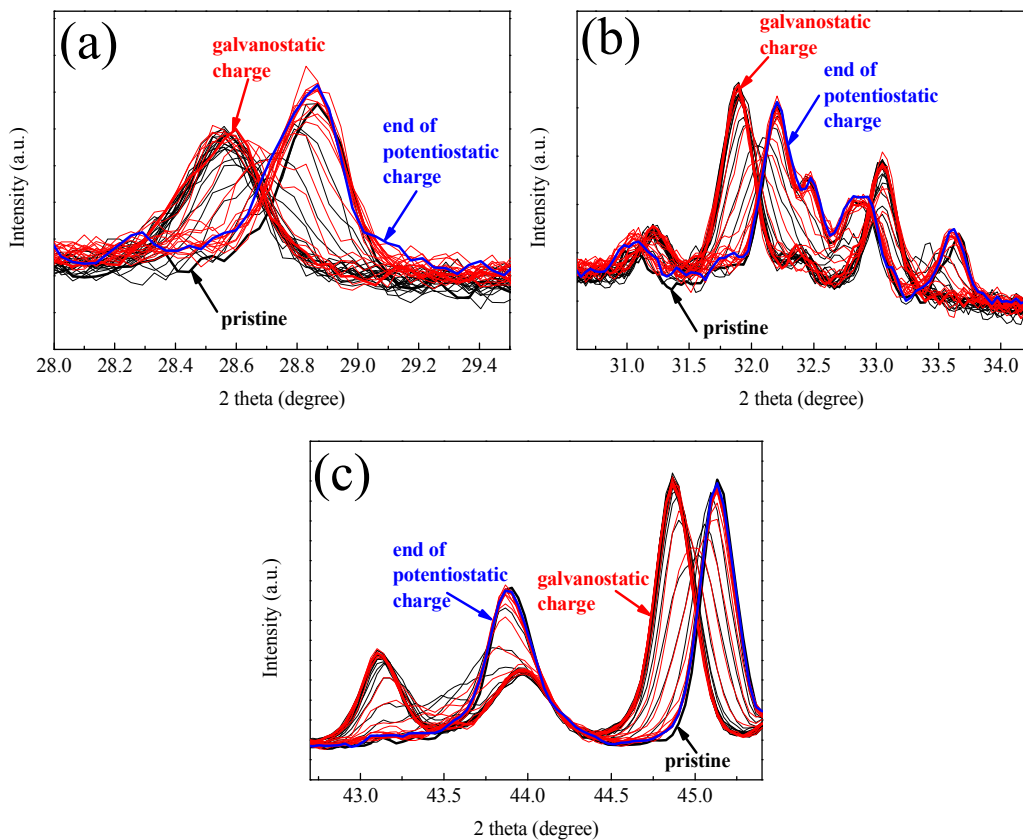


**Fig. 10.** Selected In situ XRD patterns of  $\text{Li}_{1.95}\text{Na}_{2.05}\text{Ti}_6\text{O}_{14}$  with the same background.

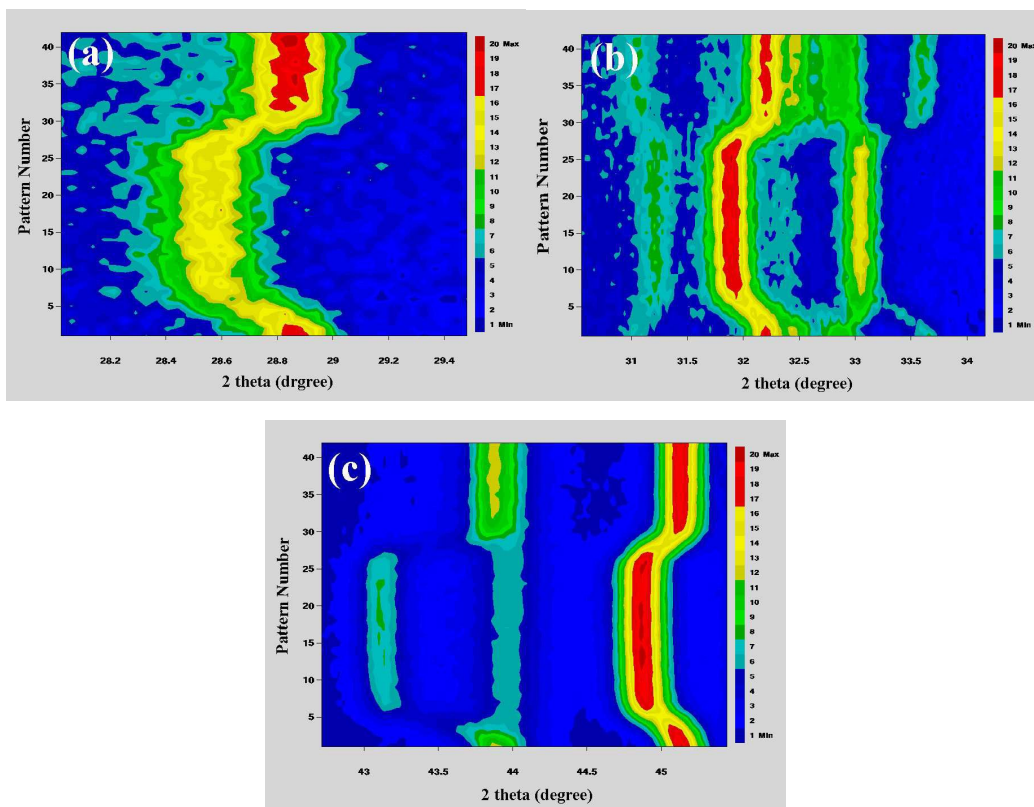


**Fig. 11.** The evolution of relative intensity versus Bragg position of  $\text{Li}_{1.95}\text{Na}_{2.05}\text{Ti}_6\text{O}_{14}$  during the charge/discharge process.

**Table 1.** Potentials of the redox peaks in the CVs for  $\text{Li}_{2-x}\text{Na}_{2+x}\text{Ti}_6\text{O}_{14}$  ( $0 \leq x \leq 0.20$ )

samples.

Samples	$\phi_{pa}$ (V)	$\phi_{pc}$ (V)	$\Delta\phi_p$ (mV) <sup>a</sup>
$\text{Li}_2\text{Na}_2\text{Ti}_6\text{O}_{14}$	1.360	1.178	182
$\text{Li}_{1.95}\text{Na}_{2.05}\text{Ti}_6\text{O}_{14}$	1.362	1.205	157
$\text{Li}_{1.9}\text{Na}_{2.1}\text{Ti}_6\text{O}_{14}$	1.355	1.190	165
$\text{Li}_{1.85}\text{Na}_{2.15}\text{Ti}_6\text{O}_{14}$	1.362	1.198	164
$\text{Li}_{1.8}\text{Na}_{2.2}\text{Ti}_6\text{O}_{14}$	1.354	1.186	168

<sup>a</sup>  $\Delta\phi_p = \phi_{pa} - \phi_{pc}$

**Table 2.** The  $\text{Li}^+$  diffusion coefficients calculated from EIS patterns for  $\text{Li}_{2-x}\text{Na}_{2+x}\text{Ti}_6\text{O}_{14}$  ( $0 \leq x \leq 0.20$ ) samples.

Samples	x=0.00	x=0.05	x=0.10	x=0.15	x=0.20
$D_{\text{Li}} (\text{cm}^2 \text{s}^{-1})$	$1.57 \times 10^{-15}$	$1.11 \times 10^{-14}$	$1.13 \times 10^{-14}$	$2.81 \times 10^{-15}$	$4.37 \times 10^{-15}$
$\sigma (\Omega \text{s}^{-0.5})$	615.5	226.5	229.2	460.1	368.6

## Graphical Abstract

Enhanced lithium storage property of Na-doped  $\text{Li}_2\text{Na}_2\text{Ti}_6\text{O}_{14}$  anode materials for secondary lithium-ion batteries

Mengmeng Lao, Peng Li, Xiaoting Lin, Lianyi Shao, Miao Shui, Nengbing Long, Dongjie Wang, Jie Shu\*

Submitted to *RSC Advances*

